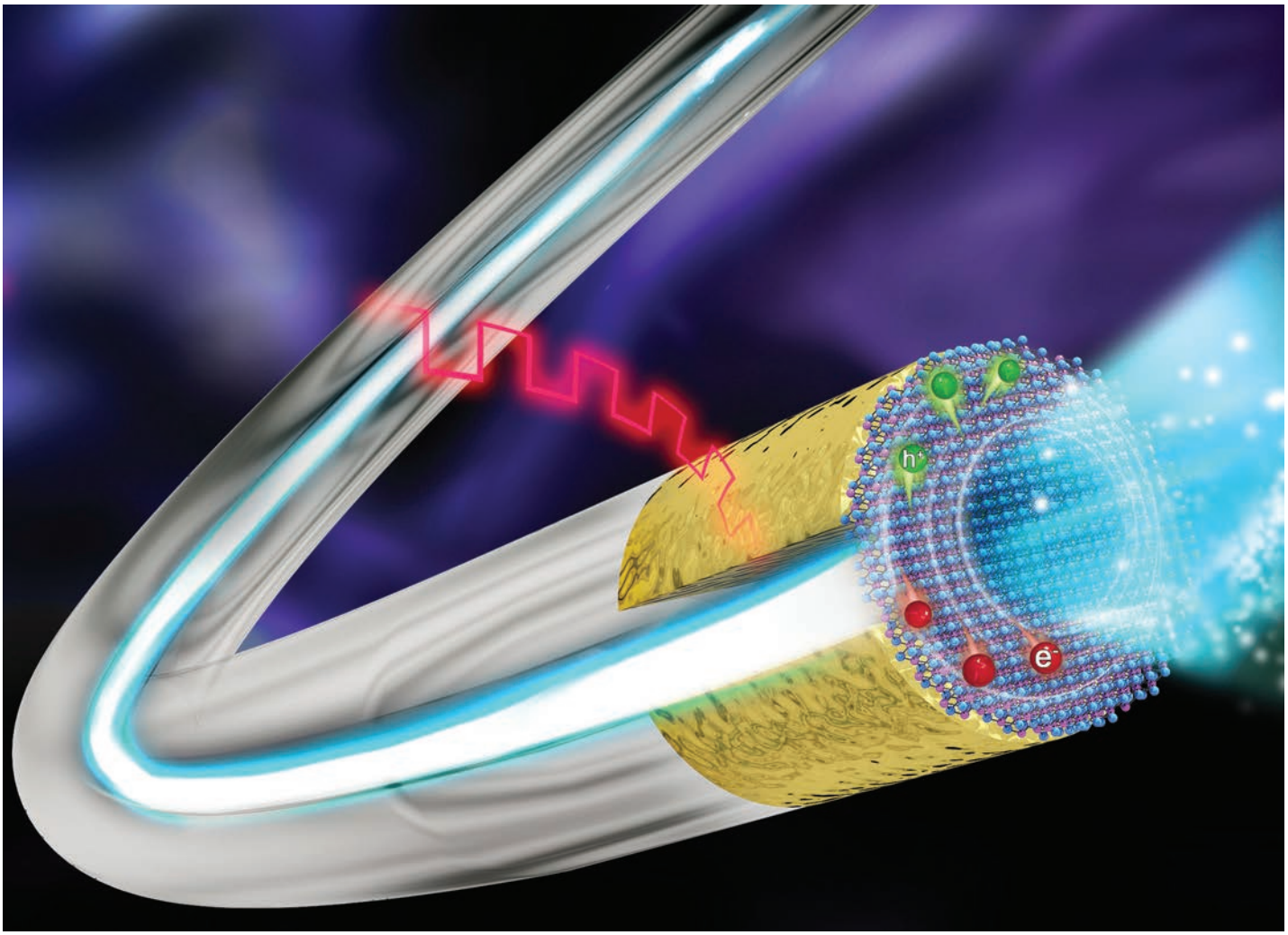

Showcasing work from National Laboratory of Solid State Microstructures, College of Engineering and Applied Sciences and Collaborative Innovation Center of Advanced Microstructures, Nanjing University, Nanjing 210093, P. R. China.

Towards an all-in fiber photodetector by directly bonding few-layer molybdenum disulfide to a fiber facet

A simple and direct way to fabricate an all-fiber in-line photodetector based on bonding MoS2 to a fiber facet is demonstrated for the first time. The fiber photodetector can work in bias-free conditions and can be integrated in fiber systems for online monitoring with low insert loss. The platform may provide a new strategy for integrating 2D material systems in fibers and actively tuning 2D materials for all-in fiber optoelectronic applications which don't require the photons to leave the fiber.

As featured in:

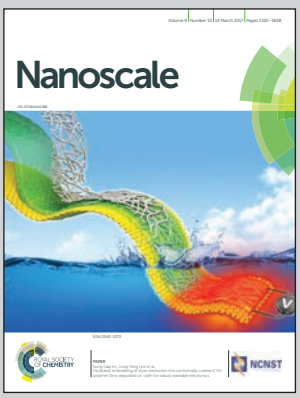

See Fei Xu *et al.*, *Nanoscale*, 2017, **9**, 3424.

ROYAL SOCIETY OF CHEMISTRY

rsc.li/nanoscale

Registered charity number: 207890

Nanoscale

PAPER

View Article Online
View Journal | View Issue

Cite this: *Nanoscale*, 2017, **9**, 3424

Towards an all-in fiber photodetector by directly bonding few-layer molybdenum disulfide to a fiber facet†

Jin-hui Chen,[a] Zhao-huan Liang,[a] Lie-rong Yuan,[b] Cheng Li,[a] Min-rui Chen,[a] Yi-dong Xia,[a] Xue-jin Zhang,[a] Fei Xu*[a] and Yan-qing Lu[a]

Received 28th October 2016,
Accepted 27th December 2016

DOI: 10.1039/c6nr08436b

rsc.li/nanoscale

Although photodetectors based on two dimensional (2D) materials have been intensively studied, there are few reports of optical fiber compatible devices. Herein we successfully fabricated an all-in fiber photodetector (FPD) based on an end-face bonded with few-layer molybdenum disulfide (MoS_2). Our FPD has a considerably high photo-responsivity of ~0.6 A W^{-1} at a bias voltage of 4 V and 0.01 A W^{-1} under the bias-free conditions. We believe that the proposed platform may provide a new strategy for the integration of 2D materials in fibers and realization of optoelectronic and sensing applications.

The invention of optical fibers[1] has lit up modern optical communication. The state-of-the-art technology has enabled ultra-low loss fibers that can transport modulated lightwave signals for approximately 100 km without the need for a repeater. However, the low-loss nature of optical fibers (made of silica), which indicates that the light–fiber interaction is very weak, limits further applications. To obtain more functional applications of optical fibers such as photodetection,[2,3] lasing,[4] and thermal detection,[5,6] researchers have tried to integrate different materials and microstructures[7] into optical fibers. Nevertheless, these platforms require a well-designed layered structure and a complex manufacturing process.[2–7]

Over the past decade, the rise of two-dimensional (2D) materials has led to many fundamental research breakthroughs[8,9] and high-performance devices.[10] Given that 2D materials are inherently compatible with fiber systems owing to their mechanical flexibility and robustness, there have been many pioneering studies that combine 2D materials, including graphene, transition metal dichalcogenides (TMDs) and topological insulators, where optical fibers realize optoelectronic[11–20] and sensing[21–26] functions. However, most of these fiber devices are passive and lack the active manipulations of 2D materials. Furthermore, there is still much potential to explore in the field of fiber integration with 2D materials. It has been proved that 2D materials can provide almost all functions required for optical communication; for example, light generation,[27–32] modulation,[33–36] and detection.[37–41] Among these, as far as we know, there are only a few studies that report on all-in fiber photodetection.[18]

Herein, we successfully fabricate an all-in fiber photodetector (FPD) by directly bonding a piece of molybdenum disulfide (MoS_2) to a fiber facet with a high photoresponsivity of ~0.6 A W^{-1} at 4 V and ~0.01 A W^{-1} at 0 V bias for light with a wavelength of 400 nm. Notably, a facile method is developed to fabricate electrodes on fibers with relatively high precision without any conventional lithographic process. Our configuration is simple, cost-effective, and can be readily extended to other 2D materials. We believe that our platform may provide a new strategy for the integration of fibers with 2D material systems and tuning of 2D materials actively for multifunctional applications.

Our FPD is illustrated in Fig. 1a. A thin layer of MoS_2 is directly bonded to the end face of an optical fiber with two gold electrodes, as is clearly shown in the Fig. 1a inset. The mechanisms of photocurrent generation can be classified as photoconductive, photovoltaic, and photothermal effects.[41] In our configuration, we adopt the photoconductive mechanism. In a photoconductive device, in the dark, the bias voltage induces a certain amount of electric flow. When the device is illuminated with photons whose energies are greater than the band gap of the semiconductor, the photon absorption generates extra electron–hole pairs, which are separated by a bias field and are collected by the electrodes. The input light power can be measured by detecting the net photocurrent. It should be noted that we selected MoS_2 as the photoconductive layer because the large band gap of MoS_2 can guarantee low dark current and good photodetection performance.[42–44]

[a]*National Laboratory of Solid State Microstructures, College of Engineering and Applied Sciences and Collaborative Innovation Center of Advanced Microstructures, Nanjing University, Nanjing 210093, P. R. China. E-mail: feixu@nju.edu.cn*
[b]*School of Physics, Nanjing University, Nanjing 210093, P. R. China*
†Electronic supplementary information (ESI) available. See DOI: 10.1039/c6nr08436b

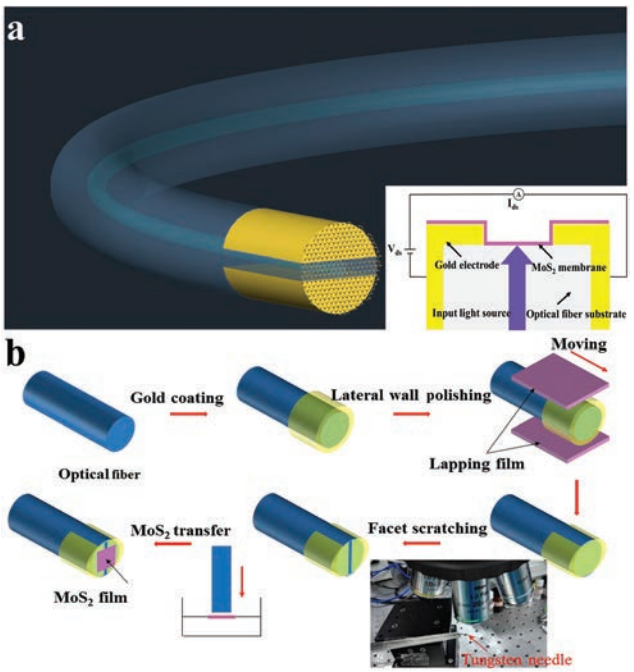

Fig. 1 Schematic of the FPD and its fabrication process. (a) The photodetection part of the FPD is integrated on the fiber facet, which is composed of a gold electrode pair and few-layer MoS_2. The MoS_2 is deposited above the electrodes. The inset is the cross-sectional part of the FPD. (b) Sequential fabrication process of the FPD. The inset shows the scratching method using a tapered tungsten probe under an optical microscope.

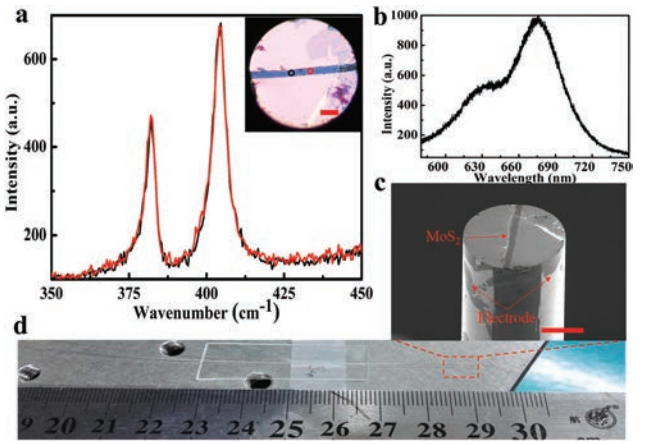

Fig. 2 Characterization of the FPD. (a) The *in situ* Raman spectra of few-layer MoS_2 in the FPD. The red and black curves are two typical spectra of the MoS_2 in the FPD, corresponding to red and black circled positions in the inset. Inset: the optical microscope image of the FPD, where the red and black circles are the selected areas for the Raman characterization. Scale bar, 20 μm. (b) The *in situ* PL spectrum of the MoS_2 in the FPD for 532 nm excitation. (c) The SEM image of the FPD. Scale bar, 50 μm. (d) Camera image of the as-fabricated FPD.

Fig. 1b demonstrates the sequential fabrication process of the FPD. Initially, to realize the FPD, a cleaved single-mode optical fiber (SMF-28, Corning, New York, USA) was deposited with a ~30 nm gold film covering all over the fiber (see the ESI† for details). The reason why we choose SMF-28 fiber is that it is the most popular optical fiber for optical communication application. Although it is designed for single mode transmission in the infrared band, it can also be used in the visible band only at the cost of multi-mode transmission with negligible loss (short distance). Then, we used two pieces of lapping films (LF1P, Thorlabs) to remove a portion of the gold layer in the lateral portion of the fiber and left two parallel gap structures (Fig. S1†). After that, we employed a tapered tungsten needle to scratch the gold layer on the end surface of the fiber to obtain a small channel corresponding to the lateral gaps. The fabrication process was accompanied by optical microscopy and a high precision moving stage (NanoMax, Thorlabs). In this way, a fiber with two separated electrodes was fabricated and the channel length and position on the end face of the fiber could be well controlled (Fig. S2†). The MoS_2 layer on mica, fabricated by chemical vapor deposition (CVD, Six Carbon Technology, Shenzhen, China) was transferred to deionized water for readiness. Finally, we adopted a dip-coating method[21,26] to transfer the MoS_2 to the fiber facet. Fig. 2(c and d) shows the structure and morphology of the prepared sample. The clear SEM image of the MoS_2 integrating fiber structure (Fig. S4†) illustrates the uniformity of the transferred film. We figure that it is because the gold has a strong affinity for chalcogenides, especially for the sulfur atoms. It is found that gold can form a semicovalent bond with sulfur, the bond strength of which is as large as 45 kcal mol^{-1}.[45] As a result, the large electrode pad on the fiber can assist smooth film transfer in the dip-coating process.

Fig. 2a shows the Raman spectra of the transferred MoS_2 film on the FPD (see the ESI† for details). It can be seen that the two selected areas' Raman fingerprints almost overlap each other, which indicates the high uniformity of the MoS_2. Using the Lorentz fitting method, the wavenumbers of the A_{1g} and E^1_{2g} modes are calculated to be 404.2 cm^{-1} and 381.9 cm^{-1}, respectively. The energy difference between the two Raman peaks is 22.3 cm^{-1}, corresponding to trilayer MoS_2.[46,47] We also measured the photoluminescence (PL) spectrum of the MoS_2, as illustrated in Fig. 2b. Two prominent peaks can be observed in the PL spectra at ~677 nm and ~626 nm, which can be attributed to A and B excitons of the MoS_2.[43] The relatively strong PL signal shows that the MoS_2 should have a few layers, which is consistent with the Raman results. It is convenient to characterize the extinction spectrum of the FPD. Fig. S6† shows a relatively long absorption tail (~1000 nm) and strong absorption when the light wavelength is shorter than 450 nm.[43,48] As a result, it may be expected that our FPD can have a high performance in short wavelengths,[42–44] which will be discussed in the next section.

To characterize the performance of photodetectors based on 2D materials, most researchers have to use an objective lens to focus the light source into a sub-sample size scale.[37,41–43] In our case, we do not need any lens system, thanks to the all-in fiber structure. The fiber waveguide can serve as a light power concen-

trator and theoretically, all the input power can be projected to the FPD. For the photoelectrical characterization, we used a reference optical power-meter (S150C, Thorlabs) to calibrate the input light power (Fig. S7†). In our FPD, the collecting electrode is positioned related to the waveguiding center (fiber core) and the gap between them is the key parameter that influences the performance of the FPD. Herein we choose the gap width as ~7.5 μm, with the gap center nearly on the fiber center position, given that it matches well with the optical modes in the fiber, which is beneficial for an efficient photodetection (Fig. S4 and S5†).

Fig. 3a shows the nonlinear *I–V* curves of the FPD in the dark, which indicates that the contact between the gold electrode and MoS_2 is not ohmic. By using the transfer length method,[49] the measured contact resistance is found to be ~48 GΩ μm and the sheet resistance of MoS_2 is ~10 GΩ $\square^{-1}$ (Fig. S8†), which is similar to the previously reported CVD MoS_2.[50] The high contact resistance can be attributed to the large sheet resistance and the Schottky barrier because of the work function mismatch.[51] When the FPD is illuminated with a 400 nm light source (MDL-III-400, CNI, China), the drain current increases due to the creation of photocarriers. The photocurrent ($I_{ph} = I_{light} - I_{dark}$) increases with the bias voltage due to the increase of the carrier drift velocity. Fig. 3b illustrates the photocurrent mapping related to the bias voltage and input light power. Qualitatively, the photocurrent saturates at a lower light power with a higher bias voltage. The photoresponsivity is one of the most important figures of merit for a photodetector, which is defined as $R = I_{ph}/P_{light}$, where P_{light} is the total incident power on the device, rather than the absorbed light power. Fig. 3c shows the photoresponsivity of the FPD related to the bias voltage at a fixed power. Intuitively, the photoresponsivity increases with the increase of the bias. It is known that for most 2D materials the photoresponsivity is highly dependent on the power due to trap states,[41,44,52] as illustrated in Fig. 3d. The trap states can greatly enhance the responsivity of MoS_2 for either increasing the photocarriers' life time or the photogating effects. As the input light power increases, the trap states are full-filled, and the gain is decreased, thus the responsivity is also decreased. The best photoresponsivity of our FPD is ~0.6 A W^{-1} with a projected light power of ~4.4 nW. Much higher responsivity can be expected if weaker light is illuminated. Although this value is much lower than the MoS_2 state-of-the-art photodetector,[41] it is reasonably high considering our gating-free conditions and relatively simple configuration (see the ESI† for the comparison of our FPD's performance with a chip based MoS_2 photodetector). Besides, it is superior to that of commercial silicon photodetectors and is two orders of magnitude larger than that of graphene-microfiber devices.[18] We also measured the performance of the FPD at 532 nm, the responsivity of which was comparable with the 400 nm light source (Fig. S9†).

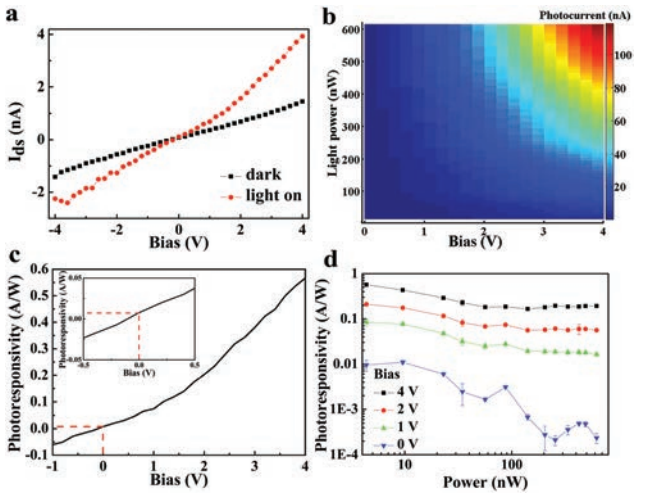

Fig. 3 Photoelectrical characterization of the FPD. (a) The *I–V* curve of the FPD in a dark environment and with light (4.37 nW @ 400 nm). (b) The photocurrent generation is related to the input light power and bias voltage. (c) The photoresponsivity of the FPD is correlated to the bias voltage with a light power of 4.37 nW. Inset: the partial enlarged view of photoresponsivity around zero bias. (d) The photoresponsivity of the FPD is related to the input power and bias voltage.

Surprisingly, our FPD can also work under bias-free conditions, as shown in the Fig. 3c inset and Fig. 3d, and the best photoresponsivity is as high as 0.01 A W^{-1}. The possible mechanism is the spatial asymmetry of electrodes, which has been used to realize bias-free graphene photodetectors.[38] We figure that the gold electrode pair is not precisely symmetric to the fiber core (light source position) due to the simple scratching technique. Thus the asymmetric interaction of the optical field and built-in electric field at the contact regions of the electrodes and MoS_2 leads to the absence of cancellation in the net photocurrent at zero bias (see the ESI† for detailed discussions). The external quantum efficiency (EQE) is used to characterize the efficiency of the impinging photons in generating charge carriers, which is closely related to the photoresponsivity:

$$\mathrm{EQE} = R\frac{hc}{e\lambda} \quad (1)$$

where h is Planck's constant, c is light speed in a vacuum, e is the electron voltage, and λ is the light wavelength. From Fig. 3d, we can calculate that the maximized EQE is ~180% for ~4.4 nW input. Considering that only part of the light power (~45%) is absorbed in the MoS_2 (Fig. S6†), the trap states in the MoS_2 should dominate in our FPD.[37,44] Although the trap states can add to the carrier life time, increasing the photon gain, they also reduce the response speed of our FPD, which is discussed below.

The photo-switching characteristics and stability of our FPD were investigated. The drain current increases to a high value under illumination and decreases to a low value under the dark conditions. We measured three different illuminated light powers, as shown in Fig. 4a, and the photocurrent dynamics were almost the same. Moreover, the stability of this switching behavior was also manifested by applying periodic ON–OFF operations of the light source, as illustrated in Fig. 4a. However, the response speed of our FPD is relatively

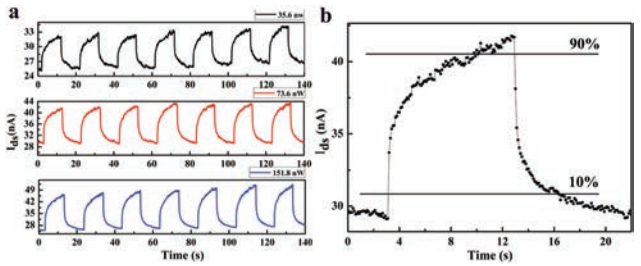

Fig. 4 Photocurrent dynamics and stability characterization. (a) Time-resolved photoresponsivity of the FPD recorded for different light powers with a bias voltage of 3 V. The laser is repeatedly turned on for a period of 10 s and turned off for 10 s. (b) An enlarged one-cycle view of the photocurrent dynamics of the FPD with a 3 V bias for 73.6 nW light power.

low. The 10%–90% rise/fall times are ~7.1 s and 3.5 s respectively as shown in Fig. 4b, which are comparable with those in previous reports.[44,53] To some extent, the response speed competes with the photoresponsivity of the photodetector. As is mentioned, the trap states dominate in our FPD. The photoresponsivity is considerably good, and as a result, the response speed is compromised. This problem can be solved if we use better-quality MoS_2 (*e.g.*, low defect density and high carrier mobility) or engineer the MoS_2-substrate interfacial properties[32,54] to reduce the charged trap density.

Conclusions

In summary, we propose and demonstrate a new all-in FPD based on few-layer MoS_2. Different from a conventional photodetector built on a silicon chip, our FPD is highly compatible with current optical fiber systems for in-line optical power monitoring. It achieves a considerably high photoresponsivity of ~0.6 A W^{-1} at 4 V for 400 nm-wavelength light. The performance of our FPD can be further improved by interface engineering and electrostatic gating,[42–44] although the complexity of the device is compromised. The chemical route to modifying the MoS_2's quality and hybrid plasmonic structure is also a promising way to enhancing the device's performance.[32,55] Our FPD can also work under bias-free conditions with photoresponsivity as high as ~0.01 A W^{-1} owing to the unintentional spatially asymmetric electrodes. This value can be enhanced if we carefully design the electrode structure and use more powerful fabrication techniques, such as focused ion beam (FIB). Although our FPD can only work in the visible band owing to the band gap limit of MoS_2, it is very promising that our platform can be extended to the infrared spectrum by employing other 2D materials, such as graphene[38,40] and black phosphorus.[39] Moreover, by using the dip-coating method, theoretically, we can obtain vertical van der Waals heterostructures in fibers, which adds another dimension to fibers integrated with 2D materials. We believe that our platform may provide a new way for the integration of 2D material systems in fibers and movement towards tuning of 2D materials actively in fibers for multifunctional applications.

Acknowledgements

This work is sponsored by the National Natural Science Foundation of China (61225026, 61535005, 61490714 and 61475069). The authors thank Cai-song Hua for his assistance in drawing the schemes.

References

1 C. K. Kao, *Rev. Mod. Phys.*, 2010, **82**, 2299.
2 M. Bayindir, F. Sorin, A. F. Abouraddy, J. Viens, S. D. Hart, J. D. Joannopoulos and Y. Fink, *Nature*, 2004, **431**, 826–829.
3 A. C. Bedeloglu, A. Demir, Y. Bozkurt and N. S. Sariciftci, *Text. Res. J.*, 2010, **80**, 1065–1074.
4 O. Shapira, K. Kuriki, N. D. Orf, A. F. Abouraddy, G. Benoit, J. F. Viens, A. Rodriguez, M. Ibanescu, J. D. Joannopoulos and Y. Fink, *Opt. Express*, 2006, **14**, 3929–3935.
5 M. Bayindir, O. Shapira, D. Saygin-Hinczewski, J. Viens, A. F. Abouraddy, J. D. Joannopoulos and Y. Fink, *Nat. Mater.*, 2005, **4**, 820–825.
6 M. Bayindir, A. F. Abouraddy, J. Arnold, J. D. Joannopoulos and Y. Fink, *Adv. Mater.*, 2006, **18**, 845–849.
7 A. Abouraddy, M. Bayindir, G. Benoit, S. Hart, K. Kuriki, N. Orf, O. Shapira, F. Sorin, B. Temelkuran and Y. Fink, *Nat. Mater.*, 2007, **6**, 336–347.
8 A. K. Geim and K. S. Novoselov, *Nat. Mater.*, 2007, **6**, 183–191.
9 A. C. Neto, F. Guinea, N. M. Peres, K. S. Novoselov and A. K. Geim, *Rev. Mod. Phys.*, 2009, **81**, 109.
10 F. Bonaccorso, Z. Sun, T. Hasan and A. Ferrari, *Nat. Photonics*, 2010, **4**, 611–622.
11 Q. Bao, H. Zhang, Y. Wang, Z. Ni, Y. Yan, Z. X. Shen, K. P. Loh and D. Y. Tang, *Adv. Funct. Mater.*, 2009, **19**, 3077–3083.
12 H. Zhang, D. Tang, L. Zhao, Q. Bao and K. Loh, *Opt. Express*, 2009, **17**, 17630–17635.
13 K. Wang, J. Wang, J. Fan, M. Lotya, A. O'Neill, D. Fox, Y. Feng, X. Zhang, B. Jiang and Q. Zhao, *ACS Nano*, 2013, **7**, 9260–9267.
14 C. Zhao, Y. Zou, Y. Chen, Z. Wang, S. Lu, H. Zhang, S. Wen and D. Tang, *Opt. Express*, 2012, **20**, 27888–27895.
15 S. Wang, H. Yu, H. Zhang, A. Wang, M. Zhao, Y. Chen, L. Mei and J. Wang, *Adv. Mater.*, 2014, **26**, 3538–3544.
16 Q. Bao, H. Zhang, B. Wang, Z. Ni, C. H. Y. X. Lim, Y. Wang, D. Y. Tang and K. P. Loh, *Nat. Photonics*, 2011, **5**, 411–415.
17 W. Li, B. Chen, C. Meng, W. Fang, Y. Xiao, X. Li, Z. Hu, Y. Xu, L. Tong and H. Wang, *Nano Lett.*, 2014, **14**, 955–959.
18 X. Sun, C. Qiu, J. Wu, H. Zhou, T. Pan, J. Mao, X. Yin, R. Liu, W. Gao and Z. Fang, *Opt. Express*, 2015, **23**, 25209–25216.
19 X. Gan, C. Zhao, Y. Wang, D. Mao, L. Fang, L. Han and J. Zhao, *Optica*, 2015, **2**, 468–471.
20 E. J. Lee, S. Y. Choi, H. Jeong, N. H. Park, W. Yim, M. H. Kim, J.-K. Park, S. Son, S. Bae and S. J. Kim, *Nat. Commun.*, 2015, **6**, 6851.

21 J. Ma, W. Jin, H. L. Ho and J. Y. Dai, *Opt. Lett.*, 2012, **37**, 2493–2495.
22 Y. Wu, B. Yao, A. Zhang, Y. Rao, Z. Wang, Y. Cheng, Y. Gong, W. Zhang, Y. Chen and K. Chiang, *Opt. Lett.*, 2014, **39**, 1235–1237.
23 J. Ma, H. Xuan, H. L. Ho, W. Jin, Y. Yang and S. Fan, *IEEE Photonics Technol. Lett.*, 2013, **10**, 932–935.
24 J. Zhang, G. Liao, S. Jin, D. Cao, Q. Wei, H. Lu, J. Yu, X. Cai, S. Tan and Y. Xiao, *Laser Phys. Lett.*, 2014, **11**, 035901.
25 S. C. Yan, B. C. Zheng, J. H. Chen, F. Xu and Y. Q. Lu, *Appl. Phys. Lett.*, 2015, **107**, 053502.
26 B. C. Zheng, S. C. Yan, J. H. Chen, G. X. Cui, F. Xu and Y. Q. Lu, *Laser Photonics Rev.*, 2015, **9**, 517–522.
27 K. F. Mak, C. Lee, J. Hone, J. Shan and T. F. Heinz, *Phys. Rev. Lett.*, 2010, **105**, 136805.
28 A. Splendiani, L. Sun, Y. Zhang, T. Li, J. Kim, C.-Y. Chim, G. Galli and F. Wang, *Nano Lett.*, 2010, **10**, 1271–1275.
29 Y. Ye, Z. Ye, M. Gharghi, H. Zhu, M. Zhao, Y. Wang, X. Yin and X. Zhang, *Appl. Phys. Lett.*, 2014, **104**, 193508.
30 S. Wu, S. Buckley, J. R. Schaibley, L. Feng, J. Yan, D. G. Mandrus, F. Hatami, W. Yao, J. Vučković and A. Majumdar, *Nature*, 2015, **520**, 69–72.
31 Y. Ye, Z. J. Wong, X. Lu, X. Ni, H. Zhu, X. Chen, Y. Wang and X. Zhang, *Nat. Photonics*, 2015, **9**, 733.
32 M. Amani, D.-H. Lien, D. Kiriya, J. Xiao, A. Azcatl, J. Noh, S. R. Madhvapathy, R. Addou, K. Santosh and M. Dubey, *Science*, 2015, **350**, 1065–1068.
33 M. Liu, X. Yin, E. Ulin-Avila, B. Geng, T. Zentgraf, L. Ju, F. Wang and X. Zhang, *Nature*, 2011, **474**, 64–67.
34 B. Sensale-Rodriguez, R. Yan, M. M. Kelly, T. Fang, K. Tahy, W. S. Hwang, D. Jena, L. Liu and H. G. Xing, *Nat. Commun.*, 2012, **3**, 780.
35 C. T. Phare, Y.-H. D. Lee, J. Cardenas and M. Lipson, *Nat. Photonics*, 2015, **9**, 511–514.
36 Z. Sun, A. Martinez and F. Wang, *Nat. Photonics*, 2016, **10**, 227–238.
37 G. Konstantatos, M. Badioli, L. Gaudreau, J. Osmond, M. Bernechea, F. P. G. de Arquer, F. Gatti and F. H. Koppens, *Nat. Nanotechnol.*, 2012, **7**, 363–368.
38 X. Gan, R.-J. Shiue, Y. Gao, I. Meric, T. F. Heinz, K. Shepard, J. Hone, S. Assefa and D. Englund, *Nat. Photonics*, 2013, **7**, 883–887.
39 N. Youngblood, C. Chen, S. J. Koester and M. Li, *Nat. Photonics*, 2015, **9**, 247.
40 F. Xia, T. Mueller, Y.-M. Lin, A. Valdes-Garcia and P. Avouris, *Nat. Nanotechnol.*, 2009, **4**, 839–843.
41 M. Buscema, J. O. Island, D. J. Groenendijk, S. I. Blanter, G. A. Steele, H. S. van der Zant and A. Castellanos-Gomez, *Chem. Soc. Rev.*, 2015, **44**, 3691–3718.
42 Z. Yin, H. Li, H. Li, L. Jiang, Y. Shi, Y. Sun, G. Lu, Q. Zhang, X. Chen and H. Zhang, *ACS Nano*, 2011, **6**, 74–80.
43 W. Choi, M. Y. Cho, A. Konar, J. H. Lee, G. B. Cha, S. C. Hong, S. Kim, J. Kim, D. Jena and J. Joo, *Adv. Mater.*, 2012, **24**, 5832–5836.
44 O. Lopez-Sanchez, D. Lembke, M. Kayci, A. Radenovic and A. Kis, *Nat. Nanotechnol.*, 2013, **8**, 497–501.
45 E. Pensa, E. Cortes, G. Corthey, P. Carro, C. Vericat, M. H. Fonticelli, G. Benitez, A. A. Rubert and R. C. Salvarezza, *Acc. Chem. Res.*, 2012, **45**, 1183–1192.
46 C. Lee, H. Yan, L. E. Brus, T. F. Heinz, J. Hone and S. Ryu, *ACS Nano*, 2010, **4**, 2695–2700.
47 K.-K. Liu, W. Zhang, Y.-H. Lee, Y.-C. Lin, M.-T. Chang, C.-Y. Su, C.-S. Chang, H. Li, Y. Shi and H. Zhang, *Nano Lett.*, 2012, **12**, 1538–1544.
48 C. Janisch, H. Song, C. Zhou, Z. Lin, A. L. Elías, D. Ji, M. Terrones, Q. Gan and Z. Liu, *2D Mater.*, 2016, **3**, 025017.
49 R. Kappera, D. Voiry, S. E. Yalcin, B. Branch, G. Gupta, A. D. Mohite and M. Chhowalla, *Nat. Mater.*, 2014, **13**, 1128–1134.
50 P.-L. Néstor, L. Zhong, R. P. Nihar, I.-R. Agustín, E. Ana Laura, M. Amber, L. Jun, M. A. Pulickel, T. Humberto, B. Luis and T. Mauricio, *2D Mater.*, 2014, **1**, 011004.
51 A. Allain, J. Kang, K. Banerjee and A. Kis, *Nat. Mater.*, 2015, **14**, 1195–1205.
52 M. M. Furchi, D. K. Polyushkin, A. Pospischil and T. Mueller, *Nano Lett.*, 2014, **14**, 6165–6170.
53 W. Zhang, J. K. Huang, C. H. Chen, Y. H. Chang, Y. J. Cheng and L. J. Li, *Adv. Mater.*, 2013, **25**, 3456–3461.
54 Z. Yu, Y. Pan, Y. Shen, Z. Wang, Z.-Y. Ong, T. Xu, R. Xin, L. Pan, B. Wang and L. Sun, *Nat. Commun.*, 2014, **5**, 5290.
55 J. Lin, H. Li, H. Zhang and W. Chen, *Appl. Phys. Lett.*, 2013, **102**, 203109.

